Hindawi Publishing Corporation
Journal of Sensors
Volume 2014, Article ID 839386, 8 pages
http://dx.doi.org/10.1155/2014/839386

Research Article

Design of a UHF Antenna for Partial Discharge Detection of Power Equipment

Youyuan Wang, Junfeng Wu, Weigen Chen, and Yajun Wang

State Key Laboratory of Power Transmission Equipment & System Safety and New Technology, Chongqing University, Chongqing 400044, China

Correspondence should be addressed to Youyuan Wang; 1028456357@qq.com

Received 23 July 2014; Revised 25 September 2014; Accepted 29 September 2014; Published 15 October 2014

Academic Editor: Tao Zhu

A single-arm Archimedean spiral antenna that can be directly fed by a 50 Ω coaxial cable is investigated in this study. Every antenna parameter is optimized under simulation to make the antenna work in the ultra-high frequency band. The influence of dielectric materials, feed cone angle, and antenna duty ratio is also examined. Partial discharge (PD) experiments on several typical artificial insulation defects are conducted, and a single-arm Archimedean spiral antenna and a typical microstrip antenna are utilized for PD measurement. The PD characteristics of different insulation defects are also analyzed. Results show that the designed antenna is suitable for ultra-high frequency monitoring. The detection sensitivity of the single-arm spiral antenna is superior to that of the ordinary microstrip antenna. The former can be utilized in wide-band measurement fields.

1. Introduction

Partial discharge (PD) detection has been applied extensively in transformer fault diagnosis and online monitoring. Latent insulation faults in transformers can be determined effectively through PD detection. Early studies have shown that the increase time of the PD pulse generated in transformer oil is very short, and the pulse width is at the nanosecond level. Thus, the electromagnetic signal caused by the PD pulse can contain the ultra-high frequency (UHF) band. The UHF signal is extracted individually to reduce the influence of noise on the PD signal. The frequency band of common electromagnetic interference is not in the range of the UHF band; thus, eliminating the interference through UHF detection is feasible. Reference [1] has demonstrated the feasibility of using the Archimedean spiral antenna to detect the UHF partial discharge signal emitted from power transformers. Several experiments have also been designed to study antenna performance. International scholars have conducted a series of studies on the Archimedean spiral antenna. The size of the Archimedean spiral antenna is reduced by changing the shape of the antenna arms or performing several complex loading techniques at the feed terminal; the antenna's performance at low frequency is improved simultaneously according to [2–6]. The radiation characteristic of the antenna is changed by transforming the overall structure of the antenna according [7, 8].

However, all of the Archimedean spiral antennas referred to above cannot eliminate the restraint of the feed balun, in which the structure increases the height of the antenna profile and the complexity of the antenna. An Archimedean spiral antenna that is fed in an unbalanced manner was proposed in 2009 by Nakano et al., who, in 2010, also proposed a single-arm Archimedean spiral antenna whose bandwidth is sufficiently wide [9, 10]. The single-arm Archimedean spiral antenna in [9] was built on a printed circuit board to make the antenna practical [11]. However, the single-arm Archimedean spiral antennas in [9, 11] do not function in the UHF band; thus, they cannot be directly applied to PD detection of power equipment. If these types of antennas are to be used, many parameters should be optimized.

A single-arm Archimedean spiral antenna designed according to UHF detection requirements is thus developed in this study. The eccentric feed method employed in [9, 11] is modified because of the change in parameters. The effects of various parameters on the antenna are discussed, and several

well-designed trials are implemented to prove the practical value of the proposed antenna.

2. Antenna Design

2.1. Working Principle. The working principle of a double-arm Archimedean spiral antenna can be explained with current band theory. If the length difference between two arms is half of the wavelength, the radiation on the adjacent spiral arms is superimposed. As a result, radiation is centered on the spiral ring belt, the circumference of which is approximately λ [12]. The working principle of a single-arm Archimedean spiral antenna can also be explained with current band theory. The difference is that the radiation is not from two antenna arms but from a single one, which eventually shortens the effective length of the antenna arm. The antenna can also achieve circular polarization with a wideband after appropriate adjustments.

2.2. Antenna Structure. The structure of the antenna is shown in Figure 1. The antenna is mainly composed of a single spiral arm, an FR4 board, a disc, and a coaxial pin. A gradually cut structure was applied to this antenna to reduce the intensity of the terminal reflected current [13]. A cone feed was utilized to improve the frequency characteristics. The antenna rotation is right-handed. More details are provided in Figure 2. The FR4 board with relative dielectric constant $\varepsilon = 4.4$ and dielectric loss $\tan\delta = 0.002$ was selected as the substrate of the antenna. The outer radius of the spiral (R_{out}) is 95.6 mm, and the inner radius (R_{in}) is 15.9 mm. The number of spiral laps (n) is 10, the antenna's arm width (w) is 3.5 mm, and the spiral growth rate (a_{sp}) is 1.267 mm/rad. The distance between the disc and spiral antenna (H) is 5 mm, and the disc radius (R_{disc}) is 30 mm.

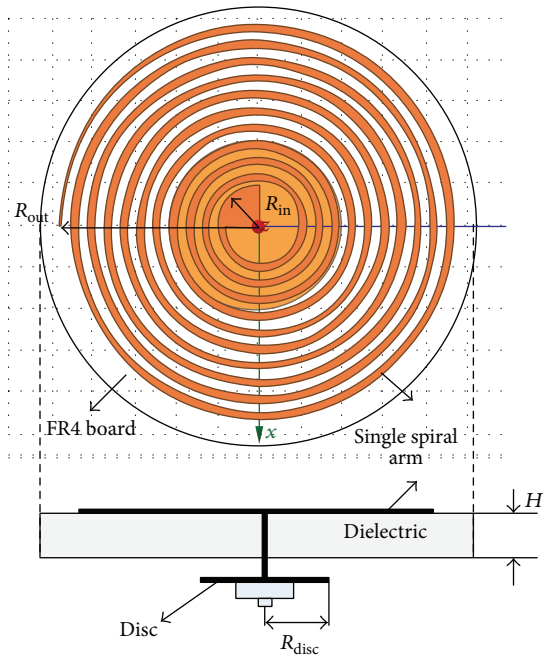

Figure 1: Schematic of the antenna structure.

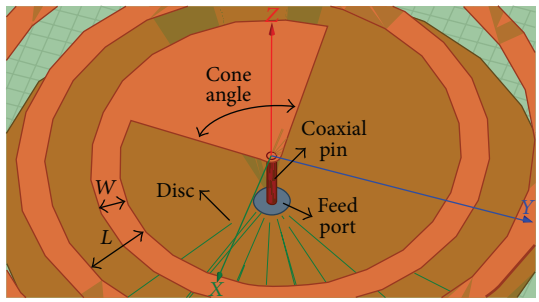

Figure 2: Feeder structure of the simulation model.

3. Simulation and Optimization

3.1. Simulation Model. The popular electromagnetic simulation software ANSYS HFSS was utilized to design the antenna. The solver is based on finite element method (FEM). To simplify the simulation process, the thin metal sheet was replaced with a 2D plane, and the boundary condition was set to perfect E. The structure of the antenna can be understood more clearly if Figures 1 and 2 are considered together. The FR4 board, whose influence on antenna performance is illustrated in the succeeding chapters, was omitted in the early simulation process. The excitation port was set to the lumped one.

3.2. Analysis of the Simulation Results. The features of the antenna were analyzed through fast sweep method, the frequency band of which is 0.5 GHz–3 GHz. As an important indicator of antenna performance, the impedance characteristic is mainly related to the impedance matching case of the antenna. VSWR and S_{11} are always utilized to value the impedance matching case in engineering [14]. If an antenna is equipped with only one port, S_{11} and reflection coefficient Γ are equal in value. The specific formulas are as follows:

$$\Gamma = S_{11} = \frac{Z_i - Z_0}{Z_i + Z_0},$$
$$\text{VSWR} = \frac{1 + |\Gamma|}{1 - |\Gamma|} = \frac{1 + |S_{11}|}{1 - |S_{11}|}, \tag{1}$$

where Z_i is the value of input impedance and Z_0 is the characteristic impedance of the feed line, the value of which is mainly 50 Ω. If impedance matching is $Z_i = Z_0$, reflection coefficient Γ becomes zero. Thus, the value of Γ or S_{11} is expected to be small.

Return loss, which is one of the output parameters of ANSYS HFSS, is also an important indicator of antenna performance. The calculation formula is

$$\text{Return Loss} = 10\lg|\Gamma|^2 = 20\lg|\Gamma| = 20\lg|S_{11}|. \tag{2}$$

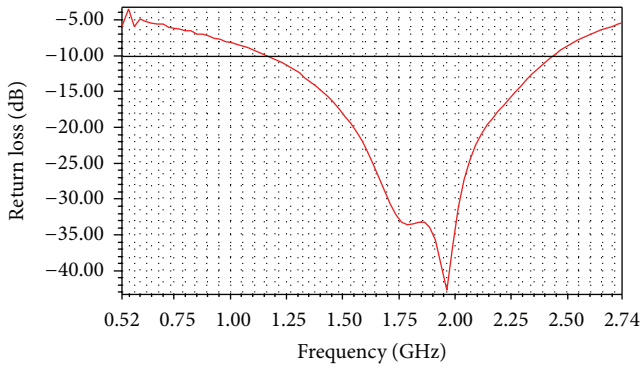

Figure 3: Frequency sweep analysis of return loss.

Figure 3 shows the relationship between antenna return loss and frequency. The return loss, which is less than −10 dB, corresponds to the frequency band 1.15 GHz–2.4 GHz. The absolute bandwidth becomes 1.25 GHz. However, the antenna performance at low or high frequency is less than expected because of the changes in the effective radiation area of the antenna. When the antenna operates at a low frequency, the radiation area is located at the edge where the effective radiation part is not long enough. If the antenna operates at a high frequency, the radiation area becomes the feed terminal, which is near the disc and coaxial pin. These factors influence antenna performance.

Directivity, which is another important performance index of the antenna, is shown in Figure 4. The figure also provides the 3D radiation pattern of the antenna operating at the frequency of 1.2 GHz. The antenna can radiate right-handed and left-handed polarized waves to both sides of the antenna plane similar to the traditional Archimedean spiral antenna. The maximum radiation directivity is at the z-axis ($\theta = 0/180^{\circ}$). Subsequent simulation shows that the radiation pattern at the x-y plane is no longer omnidirectional because the simulation frequency increases. The radiation pattern is approximately heart-shaped when the simulation frequency is 1.7 GHz. The radiation pattern becomes elliptical when the simulation frequency is 2.0 GHz.

The phenomenon referred to above is shown in Figure 5. The lobe splitting phenomenon will appear at the radiation pattern of the y-z plane if the simulation frequency continues to increase. These results suggest that the asymmetric structure of the single-arm Archimedean spiral antenna results in the asymmetric radiation pattern of the antenna. When the effective radiation area is located within the range of the bottom disc, the radiation pattern is completely affected [9]. The radius of the disc is 30 mm. Thus, if the antenna operates at a frequency of more than 1.6 GHz, the effective radiation area will be located within the range of the disc. The radiation pattern changes when the antenna operates at 1.7 and 2.0 GHz.

The double-arm Archimedean spiral antenna is a typical circular-polarization antenna, and the single-arm one can also be utilized as a circular-polarization antenna. Axial ratio is an important parameter to evaluate the performance of circular polarization. The circularly polarized bandwidth is

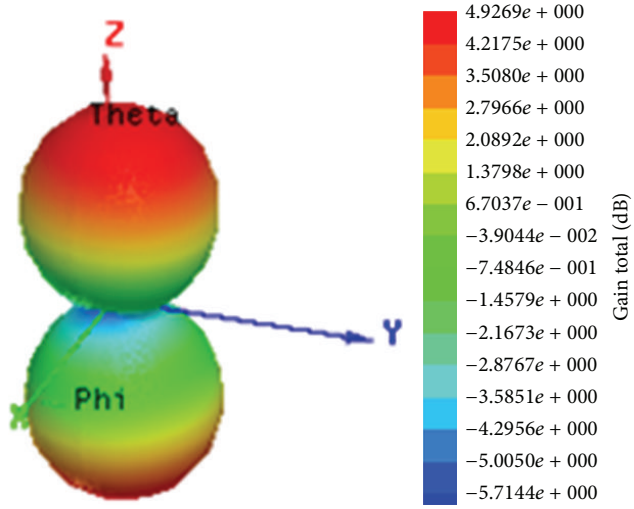

Figure 4: 3D radiation pattern of the antenna.

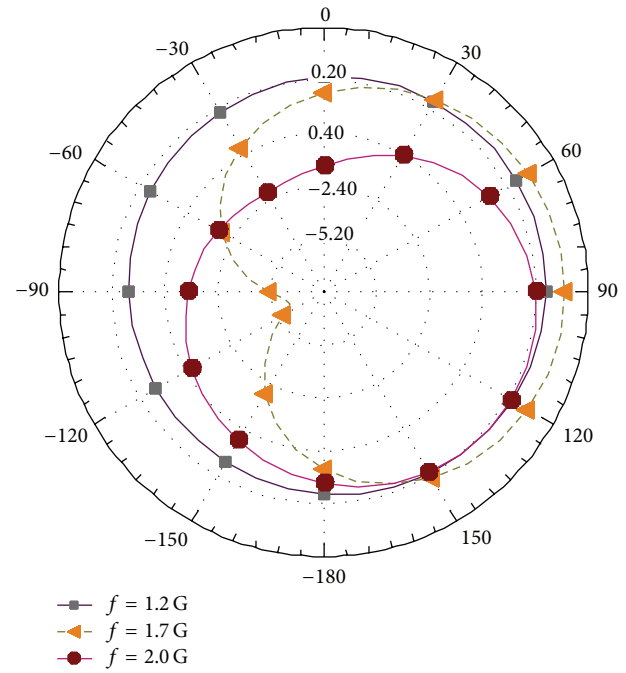

Figure 5: 2D right-handed polarized radiation pattern at the x-y plane ($\theta = 30^{\circ}$).

usually defined as the frequency range that corresponds to the axial ratio whose value is less than 3 dB. The frequency response of the antenna axis ratio is shown in Figure 6. The circularly polarized bandwidth is 0.62 GHz–2.03 GHz and basically meets the design requirement.

3.3. Impact of the Antenna Parameters. The FR4 board was replaced by air to simplify the simulation model. However, antennas are typically fabricated on a printed circuit board. Thus, analyzing the effect of dielectric materials on antenna performance is necessary. When the dielectric is changed

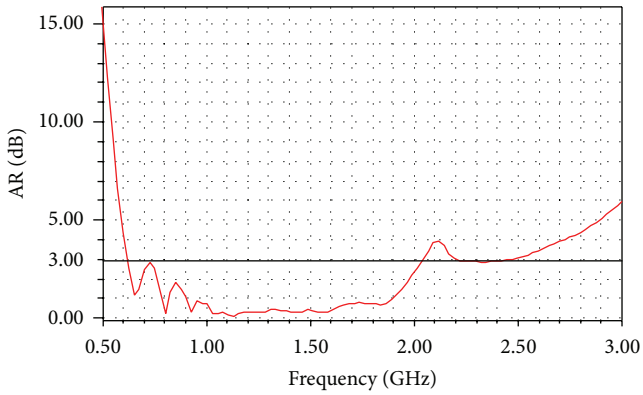

FIGURE 6: Frequency response of the antenna axis ratio.

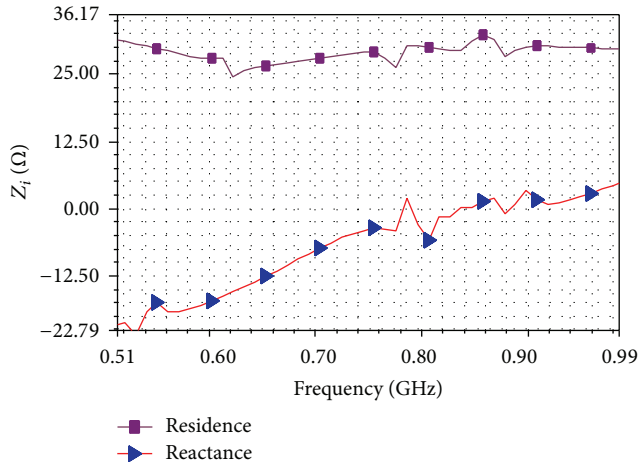

FIGURE 7: Frequency response of the antenna's input impedance.

from air to FR4, which is utilized to manufacture the printed circuit board, the frequency response of the antenna's input impedance changes immediately, as shown in Figure 7. Figure 7 also shows that the frequency band moves toward the low-frequency band, and the impedance decreases to 30 Ω. Numerous simulations have indicated that if the size of the antenna remains constant, impedance Z_i cannot be close to 50 Ω even if other parameters (except the dielectric material of the antenna) change significantly. Thus, in this study, the dielectric material used between the antenna arm and disc is not a single type. Air and FR4 comprise the material. The thickness of the FR4 board is only 1 mm, and the thickness of the air layer is 4 mm. Several insulation brackets were utilized to guarantee the mechanical connection between the antenna arm and disc. The simulation results show that the influence of the dielectric can be ignored if the thickness of the FR4 board is only 1 mm. The previous simulation conclusions can be employed in the current antenna. If the antenna works in another environment such as in the oil, or in the SF_6 gas, it is hard to calibrate the impedance changes, because the dielectric between the antenna arm and disc changes. So the antenna designed in this paper is suggested to use in the air at normal temperature.

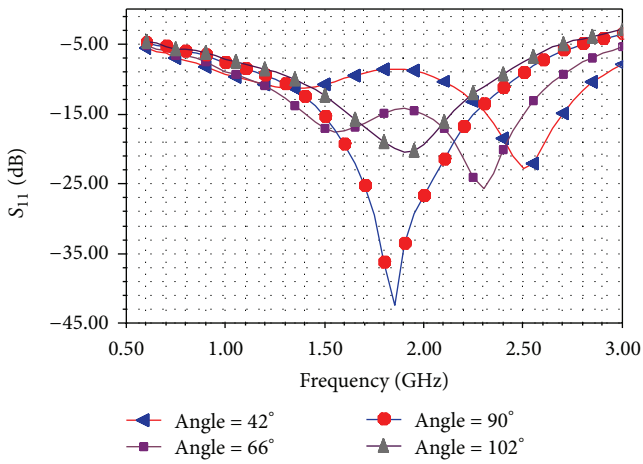

FIGURE 8: S_{11} corresponding to different cone angles.

The inner radius of the spiral antenna is much larger than the one mentioned in [11] because the working band of the antenna is included in the UHF band. If an eccentric feeding method is employed, the structure of the antenna will become unstable. Thus, a conical transition feeding method was employed to guarantee structural stability. The value of S_{11} that corresponds to different cone angles is shown in Figure 8. The return loss characteristic of the antenna is ideal when the cone angle is 90°. If the cone angle is small, the feeding transition becomes insufficient. Moreover, when the cone angle becomes too large, the current in the feeding metal sheet, which is out of the 90° range, affects the original current. Thus, the cone angle should be 90°.

The width of the antenna arm affects the coupling case of the adjacent arms. Thus, analyzing the influence caused by the antenna arm width is necessary. If the arm width (W) changes, the separation distance between the adjacent antenna arms will also change. Thus, the duty ratio, which is defined as W/L (the distance between adjacent arms), was applied to simplify the problem. Figure 9 shows the relationship between VSWR and duty ratio at a frequency of 1.9 GHz. The optimal duty ratio ranges from 0.35 to 0.5. Thus, the duty ratio was set to 0.44. The effects of other antenna parameters, such as antenna section height and disc radius, have been fully described by Nakano et al. [9] and are therefore not discussed here.

4. Partial Discharge Measurement Results and Analysis

Three typical power equipment defect models were designed to verify the detection capability of the single-arm Archimedean spiral antenna in the laboratory. A typical microstrip antenna and a pulse current detection method were also utilized to determine whether the single-arm Archimedean spiral antenna has a practical value in UHF detection.

4.1. Artificial Insulation Defect Model. Artificial insulation defect models were designed based on the models in [15].

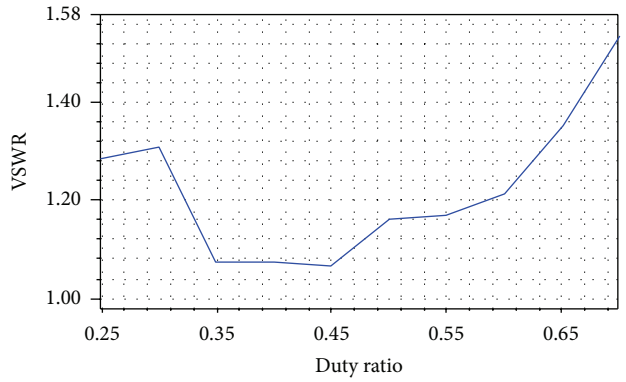

Figure 9: VSWR corresponding to different duty ratios.

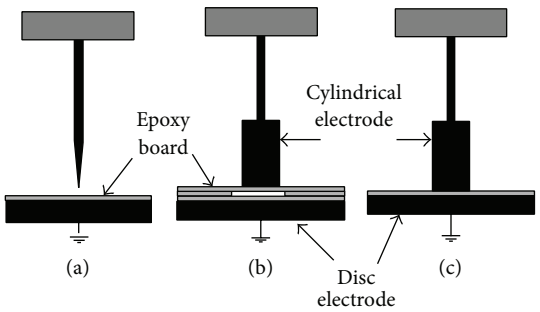

Figure 10: Three typical power equipment defect models. (a) Corona. (b) Air-gap discharge. (c) Surface discharge.

The preparation methods were adopted from [16]. The model structure is shown in Figure 10. The diameter of the cylindrical electrode is 25 mm, and the diameter of the disc electrode is 80 mm, which is equal to the diameter of the epoxy board whose thickness is 0.5 mm. The air-gap defect model consists of three epoxy boards; the middle one has a hole with a diameter of 38 mm. The curvature radius of the needle electrode utilized in the corona defect model is 200 μm, and the distance between the needle electrode and the epoxy board is approximately 3 mm. All the artificial insulation defect models were placed in glass containers filled with transformer oil to simulate the discharge in the transformer oil.

The wiring diagram is shown in Figure 11. Detection impedance was utilized to obtain the pulse current signal caused by PD. The UHF signal captured by the antennas is transported to the oscilloscope through the transmission cable. The distance of the cable is equal to the one used to transport the signal from detection impedance. The detection impedance was concatenated into the grounding line of the defect model, and the antennas were set 40 cm far away from the defect model. All the test was carried out in the shielding room whose size is 6 m × 4 m × 3.3 m. The maximal sensitivity of the single-arm Archimedean spiral antenna ranges from 3.5 dBi to 7.3 dBi when the antenna works at different frequencies.

The background noise should be measured before the test. The signal from the single-arm Archimedean spiral antenna, the signal from the typical microstrip antenna, and detection

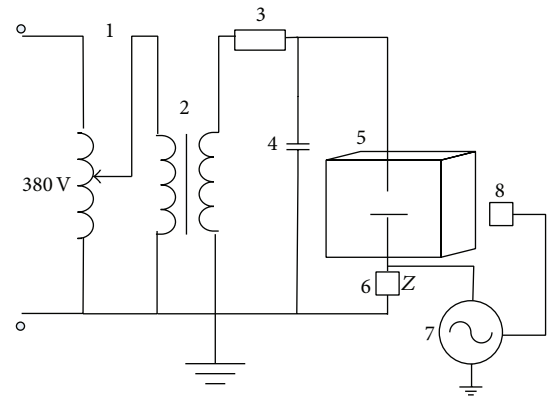

Figure 11: Experiment wiring diagram. (1) Regulator. (2) Test transformer. (3) Protection resistor. (4) Coupling capacitor. (5) Defect model. (6) Detection impedance. (7) Oscilloscope. (8) UHF antennas.

impedance were measured simultaneously. The inception discharging voltage of each defect was recorded as U_0, and the final test voltage under which the PD signal was obtained should be 1.2 U_0. The distance between the UHF antennas (including the spiral and microstrip antennas) and the defect models is 40 cm, and the length of the transmission cables is the same.

4.2. Test Results and Analysis. The background noise measured by the single-arm Archimedean spiral antenna is 1.35 mV. No significant pulse interference was observed throughout the entire test time. In addition, the background noise level remained stable. The corona discharge signal obtained by the spiral antenna and detection impedance are shown in Figure 12. The measurement result shows that the signal-to-noise ratio (SNR) of the designed antenna is satisfactory and that corona discharge always occurs at the peak value of the test voltage. Moreover, the discharge at the negative peak value is more likely to induce the UHF signal; the phenomenon can be explained through needle-plate electrode discharge theory [17]. Although PD occurs at the positive peak value, the measurement sensitivity of the spiral antenna is not sufficiently good compared with its detection impedance. The long distance between the needle and disc electrode leads to the long increase time of the positive polarity current pulse and the UHF signal, which is induced by the current pulse that attenuates at the same time [18].

Figure 13 shows the air-gap discharge signal obtained by the spiral antenna. Compared with the corona discharge in oil, the air-gap discharge appears to be more active. It always occurs in the 0°–90° and 180°–270° phases of the test voltage. Within these ranges, the absolute value of the test voltage increases. Given that gas insulation is a type of recoverable insulation, PD also disappears when the value of the voltage decreases. Thus, air-gap discharge always occurs in the 1/4 and 3/4 periods of the power frequency voltage [19].

Figure 14 shows that the PD characteristic of the surface discharge model is not obvious, and the amplitude of

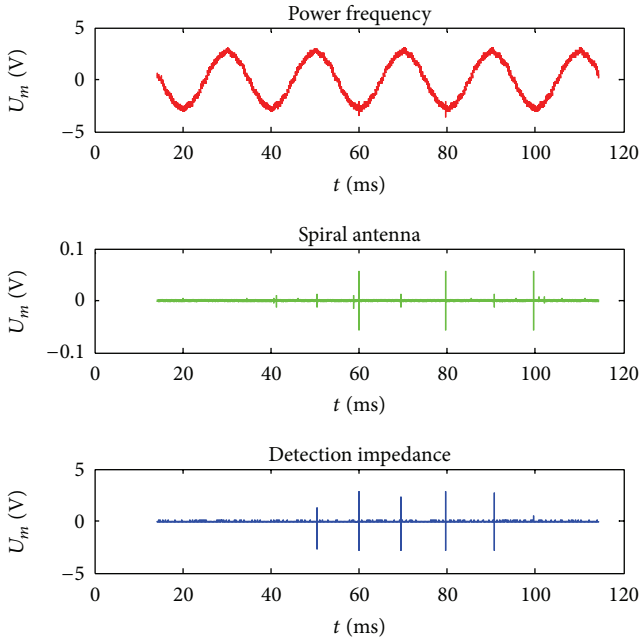

Figure 12: Corona discharge signal.

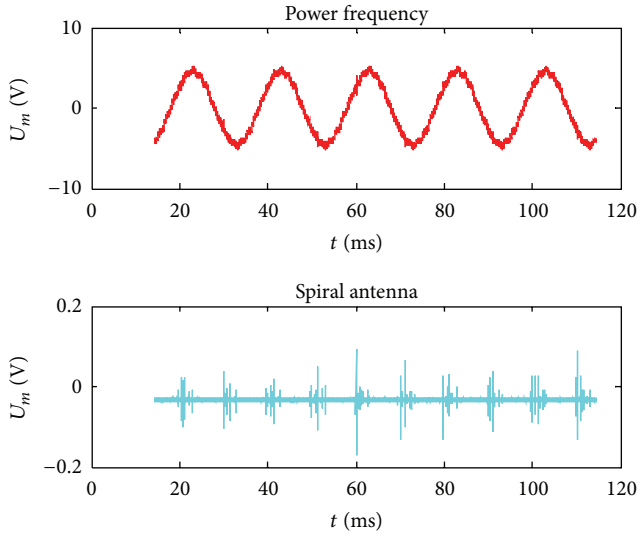

Figure 13: Air-gap discharge signal.

the signal from the detection impedance is small. The UHF signal acquired by the spiral antenna is almost covered by background noise. The development of surface discharge is relatively slow, and the experiment time is too short to obtain a good PD result [20]. Thus, the detection result of the antenna is not sufficiently good. Increasing the test time and performing signal denoising are necessary to obtain better surface discharge data.

The above analysis shows that the spiral antenna designed in this study can effectively detect the PD signals originating from the typical transformer insulation defect models. The phase characteristic of the signal is obvious. The SNR of the antenna meets the requirement of general measurement,

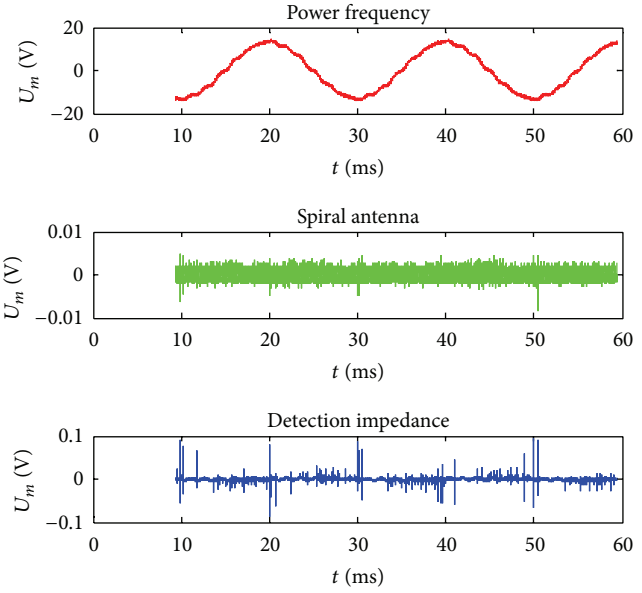

Figure 14: Surface discharge signal.

and the antenna can be utilized for UHF detection. To simulate the PD phenomenon that occurs in the power transformer accurately, the test time and artificial model should be designed reasonably.

4.3. Comparative Tests with the Microstrip Antenna. The external dimension of the microstrip antenna with center frequency of 900 MHz is 15.8 cm × 12.5 cm. Thus, the area of the microstrip antenna is close to 200 cm^2. The area of the antenna designed in this study is approximately 280 cm^2. The microstrip and spiral antennas receive the UHF signal generated by the same PD source simultaneously. The denoising function "wden" in Matlab was applied to pretreat the data. Figure 15 shows the output signal of the two antennas during one voltage cycle; the defect mode is air-gap defect. The detection sensitivity of the spiral antenna is significantly higher than that of the microstrip antenna. Although the area of the spiral antenna is slightly larger than that of the microstrip one, the sensitivity of the spiral antenna is an order of magnitude higher than that of the typical microstrip antenna. Using the spiral antenna to detect the PD signal of air-dap defect, whose energy concentration is at a frequency lower than 1 GHz, appears to be insufficient [16]. However, as long as the spiral antenna makes full use of the energy separated at a high frequency, its detection effect is better than that of a narrow band antenna.

5. Conclusion

A single-arm Archimedean spiral antenna operating at a frequency band of 1.15 GHz–2.4 GHz was designed. Its performance was studied in the laboratory. The main conclusions are as follows.

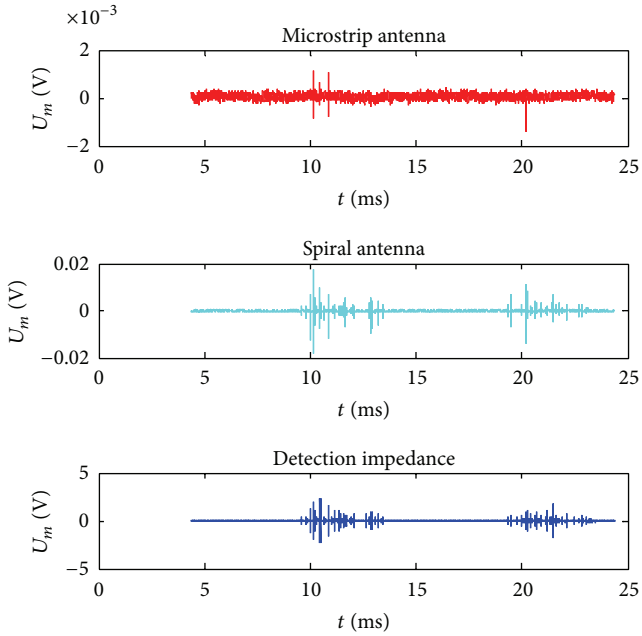

FIGURE 15: PD signal of the air-gap model during one cycle.

(1) The single-arm Archimedean spiral antenna can be directly fed by a 50 Ω coaxial cable and can operate at the ultra-high frequency band. The structure of the single-arm antenna differs from that of the single-arm one in [9].

(2) The bandwidth of the single-arm Archimedean spiral antenna is wide, and its section height is lower than that of the traditional double-arm antenna. However, compared with the double-arm antenna, the directional characteristics of the single-arm antenna are not good enough, and its surface area is larger.

(3) The single-arm Archimedean spiral antenna can detect the PD signal originating from the transformer insulation defect. The sensitivity of the antenna is significantly higher than that of a narrowband antenna and it is the first time to use the single-arm Archimedean spiral antenna in the field of PD detection.

Conflict of Interests

The authors declare that there is no conflict of interests regarding the publication of this paper.

Acknowledgment

The study is supported by the National Science Foundation of China (51321063).

References

[1] G. Wang, Y. Zheng, Y. Hao et al., "Study on the ultra-high-frequency sensor for PD detection in power transformer," *Proceedings of the CSEE*, vol. 22, no. 4, pp. 155–161, 2002.

[2] H. Li, "Analysis and design of a new-type planar Archimedean spiral antenna," *Radar and Confrontation*, no. 3, pp. 43–45, 53, 2006.

[3] Z. He, F. Xu, and J. Cui, "Design of miniaturized planar spiral satellite antenna," *Spacecraft Engineering*, vol. 21, no. 1, pp. 68–71, 2012.

[4] Z. Song, H. Li, H. Yang et al., "Study on a miniaturized meander Archimedean spiral antenna," *Journal of Microwaves*, vol. 25, no. 2, pp. 53–57, 2009.

[5] Y. Zhu, S. Zhong, S. Xu et al., "Design of miniaturized planar spiral antenna and its wideband balun," *Journal of ShangHai University: Natural Science*, vol. 14, no. 6, pp. 581–584, 2008.

[6] Y. Wang, G. Wang, and J. Liang, "Design of a Archimedean spiral antenna with low-profile," *Journal of Microwaves*, vol. 28, no. 4, pp. 5–9, 2012.

[7] N. Rahman and M. N. Afsar, "A novel modified archimedean polygonal spiral antenna," *IEEE Transactions on Antennas and Propagation*, vol. 61, no. 1, pp. 54–61, 2013.

[8] L. Li, "Design and analysis of complementary Archimedean spiral antenna," *Telemetry and Remote Control*, vol. 24, no. 04, pp. 31–36, 2003.

[9] H. Nakano, R. Satake, and J. Yamauchi, "Extremely low-profile, single-arm, wideband spiral antenna radiating a circularly polarized wave," *IEEE Transactions on Antennas and Propagation*, vol. 58, no. 5, pp. 1511–1520, 2010.

[10] H. Nakano, T. Igarashi, H. Oyanagi, Y. Iitsuka, and J. Yamauchi, "Unbalanced-mode spiral antenna backed by an extremely shallow cavity," *IEEE Transactions on Antennas and Propagation*, vol. 57, no. 6, pp. 1625–1633, 2009.

[11] Z. Liu, Z. Qian, and Z. Han, "Design of a conformal wideband circularly polarized spiral antenna," *Telecommunication Engineering*, vol. 51, no. 11, pp. 94–98, 2011.

[12] J. Kaiser, "The Archimedean two-wire spiral antenna," *IRE Transactions on Antennas and Propagation*, vol. 8, no. 3, pp. 312–323, 1960.

[13] B. Shanmugam and S. K. Sharma, "Investigations on a novel modified archimedean spiral antenna," in *Proceedings of the IEEE International Symposium on Antennas and Propagation (APSURSI '11)*, pp. 1225–1228, Spokane, Wash, USA, July 2011.

[14] L. Zhang, *Study of compact micro-strip antennas with wide-band and multi-band [M.S. thesis]*, Dept. Radio Physics, East China Normal Univ, Shanghai, China, 2005.

[15] J. Li, J.-X. Ning, Z.-R. Jin, Y.-Y. Wang, and M. Li, "Research on UHF Hilbert fractal antenna for online transformer PD monitoring," *Electric Power Automation Equipment*, vol. 27, no. 6, pp. 31–35, 2007.

[16] C. Cheng, *Study on fourth-order fractal antenna and signal processing and recognition for UHF monitoring of PDs in power transformers [M.S. thesis]*, Department of Electronic Engineering, Chongqing University, Chongqing, China, 2009.

[17] J. Kuffel, W. S. Zaengl, and E. Kuffel, *High Voltage Engineering: Fundamentals*, Butterworth-Heinemann, Oxford, UK, 2nd edition, 2000.

[18] X. H. Zhao, J. G. Yang, X. L. Lu, P. Yuan, S. Wang, and Y. M. Li, "Comparative research on current pulse method and UHF measurements of partial discharge in mineral oil," *High Voltage Engineering*, vol. 34, no. 7, pp. 1401–1404, 2008.

[19] W.-G. Chen, C. Wei, C.-X. Sun, and J. Tang, "Air-gap discharge characteristics in transformer oil-paper insulation and gas generation law," *High Voltage Engineering*, vol. 36, no. 4, pp. 849–855, 2010.

[20] W. G. Chen, J. F. Yang, Y. Ling, and X. Chen, "Surface discharge characteristics and gas generation law in oil-paper insulation of transformer," *Journal of Chongqing University*, vol. 34, no. 1, pp. 94–99, 2011.